J Neurooncol (2017) 134:433–441
DOI 10.1007/s11060-017-2545-2

CLINICAL STUDY

Differentiating radiation necrosis from tumor progression in brain metastases treated with stereotactic radiotherapy: utility of intravoxel incoherent motion perfusion MRI and correlation with histopathology

Jay S. Detsky[1,2] · Julia Keith[3] · John Conklin[2,4] · Sean Symons[4] · Sten Myrehaug[1] · Arjun Sahgal[1] · Chinthaka C. Heyn[4] · Hany Soliman[1]

Received: 4 February 2017 / Accepted: 27 June 2017 / Published online: 3 July 2017

Abstract Radiation necrosis is a serious potential adverse event of stereotactic radiosurgery that cannot be reliably differentiated from recurrent tumor using conventional imaging techniques. Intravoxel incoherent motion (IVIM) is a magnetic resonance imaging (MRI) based method that uses a diffusion-weighted sequence to estimate quantitative perfusion and diffusion parameters. This study evaluated the IVIM-derived apparent diffusion coefficient (ADC) and perfusion fraction (f), and compared the results to the gold standard histopathological-defined outcomes of radiation necrosis or recurrent tumor. Nine patients with ten lesions were included in this study; all lesions exhibited radiographic progression after stereotactic radiosurgery for brain metastases that subsequently underwent surgical resection due to uncertainty regarding the presence of radiation necrosis versus recurrent tumor. Pre-surgical IVIM was performed to obtain f and ADC values and the results were compared to histopathology. Five lesions exhibited pathological radiation necrosis and five had predominantly recurrent tumor. The IVIM perfusion fraction reliably differentiated tumor recurrence from radiation necrosis ($f_{mean} = 10.1 \pm 0.7$ vs. 8.3 ± 1.2, $p = 0.02$; cutoff value of 9.0 yielding a sensitivity/specificity of 100%/80%) while the ADC did not distinguish between the two ($ADC_{mean} = 1.1 \pm 0.2$ vs. 1.2 ± 0.4, $p = 0.6$). IVIM shows promise in differentiating recurrent tumor from radiation necrosis for brain metastases treated with radiosurgery, but needs to be validated in a larger cohort.

Keywords IVIM · Brain metastases · Radiation necrosis · MRI · Stereotactic radiosurgery

Introduction

High dose focused radiation including stereotactic radiosurgery (SRS) or fractionated stereotactic radiotherapy (FSRT) is the standard treatment for patients with limited brain metastases and good performance status [1–3]. One of the most significant late effects from SRS is radiation necrosis, which can have a significant impact on neurological function and quality of life [2]. The rate of SRS-induced radiation necrosis varies widely in the literature and largely depends on whether radiation necrosis is considered a reversible or irreversible injury, or both, to the white matter in the brain. After SRS treatment, it is difficult to clinically or radiographically determine if radiation injury is a transient or permanent change [4]. Radiographic findings consistent with radiation necrosis include a peripherally enhancing and centrally necrotic lesion on T1-weighted post-gadolinium magnetic resonance imaging (MRI) sequences and an increase in volume of enhancing lesion that is within the high dose radiosurgery volume, occurring at least 3 months after SRS [5]. These changes can be seen in up to 30% of patients treated with SRS [4, 6, 7]. Severely symptomatic radiation necrosis requiring surgical resection occurs in up to 5.5% of patients by 24 months after treatment [7].

✉ Hany Soliman
hany.soliman@sunnybrook.ca

1 Departments of Radiation Oncology, Odette Cancer Center, Sunnybrook Health Sciences Centre, 2075 Bayview Avenue, T2-187, Toronto, ON M4N3M5, Canada

2 University of Toronto, Toronto, ON, Canada

3 Department of Pathology, Sunnybrook Health Sciences Centre, Toronto, ON, Canada

4 Department of Medical Imaging, Sunnybrook Health Sciences Centre, Toronto, ON, Canada

MRI is the gold standard for diagnosing brain metastases and monitoring response to treatment. However, differentiating radiation necrosis from tumor progression using conventional MRI is difficult as both entities exhibit an increase in enhancement with or without edema and clinical symptoms. For tumor progression after SRS, salvage treatments such as surgical resection can improve overall survival [8]. Conversely, radiation necrosis can often be managed conservatively with observation, steroids, or with bevacizumab for symptomatic necrosis [9]. Therefore, the ability to distinguish between these two processes using a non-invasive imaging technique is critical to appropriately managing these patients.

Numerous advanced imaging methods have been used in an attempt to distinguish radiation necrosis from tumor recurrence, including the ratio of T2–T1 enhancement on MRI [10], diffusion weighted imaging (DWI) [11], MRI perfusion-based measurements including dynamic contrast-enhanced (DCE) [12] and dynamic susceptibility-weighted (DSC) imaging [13], magnetic resonance spectroscopy (MRS) [14], single photon emission computed tomography (SPECT) [15] and positron emission tomography (PET) using 18F-fluorodeoxyglucose (FDG) [16] and 11C-methyl-methionine [17] tracers. Few studies have correlated imaging techniques with surgical pathology and there remains no accepted radiographic method for diagnosing radiation necrosis [4]. One study showed that even with a combination of several advanced imaging techniques including perfusion CT, MRS, SPECT and PET in patients who subsequently underwent surgical resection, the preoperative neuroradiological studies proved correct in only nine of 15 patients [18].

Functional imaging with MRI including diffusion and perfusion measurements have shown promise as imaging biomarkers to characterize structural changes seen after SRS [4, 6]. Intravoxel incoherent motion (IVIM) is a method that provides quantitative diffusion and perfusion parameters via a multiple b-value diffusion-weighted MRI sequence [19]. Kim et al. recently demonstrated that IVIM diffusion and perfusion parameters were superior to DSC-based perfusion parameters alone in distinguishing recurrent tumor from treatment effect for brain metastases after SRS; this study, however, relied on longitudinal imaging and not histopathology to define outcomes [20]. IVIM has certain advantages over DSC perfusion imaging in that it does not require intravenous contrast or the estimation of an arterial input function, and provides inherent coregistration of diffusion and perfusion data [21].

The hypothesis of this study was that IVIM-based diffusion and perfusion measurements would be able to differentiate post-radiation recurrent or progressive tumor from radiation necrosis, using histopathology as the reference standard.

Methods and materials

Study population

After institutional research ethics board approval, patients who had SRS for brain metastases with a biopsy proven extracranial solid malignancy and who subsequently underwent surgical resection for presumed tumor progression or radiation necrosis between October 2014 and March 2016 were reviewed. All patients were treated with single fraction SRS via a cone-based linear accelerator system or with FSRT. For patients who had SRS, doses ranged from 18 to 20 Gy in a single fraction. FSRT was most commonly delivered in five fractions with doses ranging from 27.5 to 35 Gy.

Imaging protocol

Patients were scanned on a 3.0-T MRI system (Achieva, Philips Healthcare, Best, Netherlands) using an eight-channel phased array head coil. IVIM data was acquired using a diffusion-weighted echo-planar imaging (EPI) pulse sequence [22] with diffusion weighting along three orthogonal directions with six b-values (b = 0, 200, 400, 600, 800, 1000 s/mm^2). Axial images with a thickness of 5 mm were acquired with TR/TE 6000 ms/61 ms, NEX = 1, FOV = 24 cm, matrix = 208 × 168, in-plane resolution of 1.16 × 1.16 mm. Contrast-enhanced imaging (following administration of 0.1 mmol/kg of Gadolinium) was performed using a T1-weighted 3D gradient-echo acquisition with a resolution of 1 × 1.1 mm^2, slice thickness = 1.5 mm, NEX = 1, TR = 9.5 ms, TE = 2.3 ms, and flip angle = 8°.

Image processing and analysis

The standard IVIM biexponential model is described by the following equation [23]:

$$S(b)/S_0 = f \cdot e^{-bD^*} + (1-f) \cdot e^{-bD} \quad (1)$$

where S(b) is the signal intensity at a specific b-value, S_0 is the signal intensity at b = 0, D* is the pseudodiffusion coefficient which is related to blood flow in the microcirculation, f is the perfusion fraction (the fraction of water within a voxel that is contained within the microcirculation), and D is the diffusion coefficient related to true molecular diffusion of water. Using the simplifying assumption that D* >> D, Eq. (1) becomes:

$$\ln(S(b)/S_0) = -bD + \ln(1-f) \quad (2)$$

where the left side of the equation can be expressed as a linear relationship with slope D and intercept ln(1 − f). This simplified model has previously been validated against the

full biexponential model [24]. The apparent diffusion coefficient (ADC) was calculated using the b = 0 and b = 1000 s/mm^2 images as:

$$ADC = -\ln\left(\frac{S(1000)}{S(0)}\right)/1000 \quad (3)$$

Using the post-Gadolinium T1-weighted images, a manual region-of-interest (ROI) was generated encompassing the volume of contrast enhancement (including enhancement and any non-enhancing necrotic regions) representing either tumor or radiation necrosis. The T1-weighted images were then co-registered to the IVIM images using deformable registration (AFNI, NIH, Bethesda, MD) and the contours were transferred onto the IVIM images. The perfusion fraction (f) and apparent diffusion coefficient (ADC) were calculated on a voxel-by-voxel basis using asymptotic fitting of the data using equations (2) and (3) via linear least squares regression (Matlab, Optimization Toolbox; Mathworks, Natick, Massachusetts) [24]. The mean values for f (f_{mean}) and ADC (ADC_{mean}) as well as cumulative histogram parameters including the 90th percentile for f (f_{90}) and 10th percentile for ADC (ADC_{10}) were calculated for each lesion. These histogram parameters (f_{90} and D_{10}) have been previously shown to be more reliable than mean values for distinguishing radiation necrosis from tumor recurrence [25]. Perfusion fraction (expressed as a %) and ADC (expressed in units of 10^{-3} mm^2/s) were compared between tumors with predominantly recurrent tumor versus those with predominantly radiation necrosis using a two-tailed Student's t-test.

Histopathology

Surgical resection of the enhancing disease was performed through open craniotomy and sent for pathology review. Central pathology review was performed by an expert neuropathologist (JK) blinded to the functional imaging results. Hematoxylin and eosin-stained (H&E) slides were prepared from formalin-fixed tissue by routine processing. The relative volume of tissue composed of residual tumor cells, tumor necrosis, and radiation necrosis were quantitatively assessed. Tumor necrosis was defined as regions of coagulative necrosis in which outlines of 'ghost' tumor cells can be seen. Radiation necrosis exhibited normocellular brain parenchyma with edema, gliosis, vascular hyalinization with well circumscribed regions of bland necrosis [26].

In cases with mixed pathology, we used the definitions previously described in a study of glioblastoma multiforme (GBM) cases resected after radiation [27]: greater than 25% of the specimen composed of tumor cells represents recurrent tumor, and less than 25% represents radiation necrosis.

Results

Patient and tumor characteristics

Nine patients with ten total lesions were included in the analysis. One patient had two lesions removed in two different surgeries 4 months apart; an MRI scan with IVIM was acquired prior to each surgical resection. In all cases there was no consensus regarding the likelihood of recurrent tumor versus radiation necrosis prior to surgery. Clinical and treatment details for all ten lesions are described in Table 1. The most common primary site of disease was lung (n = 4) followed by breast (n = 3). The majority of the lesions (n = 8) were supratentorial involving the right frontal lobe (n = 4), left frontal lobe (n = 3), and right occipital lobe (n = 1). Median age of the patients was 56 years old and slightly more patients were female (n = 6) than male. Three patients were treated with single fraction radiosurgery while the other seven were treated with fractionated stereotactic radiation in five fractions (n = 6) or three fractions (n = 1).

Five of the ten lesions exhibited primarily radiation necrosis on histopathology. One case demonstrated pure radiation necrosis, while the other four cases had small islands of residual tumor cells (ranging from 5 to 20% of the specimen volume). The remaining five lesions predominantly had a combination of residual tumor and tumor necrosis and met the pre-defined criteria for recurrent tumor. Figure 1 shows the anatomical MRI (post-Gadolinium T1 image), ADC and perfusion fraction maps for a case of radiation necrosis and for recurrent tumor. Figure 2 shows a histological example of radiation necrosis next to an island of residual tumor.

Perfusion fraction (f) and ADC: differentiating tumor from radiation necrosis

Table 2 details the f_{mean}, f90, ADC_{mean}, ADC_{10}, and the histologic tumor fraction for all the lesions. Lesions with predominantly recurrent tumor had higher f_{mean} and f_{90} compared lesions with pathological radiation necrosis ($f_{mean} = 10.1 \pm 0.7$ vs. 8.3 ± 1.2, $p = 0.02$; $f_{90} = 19.8 \pm 3.8$ vs. 14.9 ± 2.5, $p = 0.047$). A cutoff value for f_{mean} of nine yields a sensitivity of 100% and specificity of 80% for identifying recurrent tumor. The one lesion with a f_{mean} over nine, that was shown histologically to be radiation necrosis, was from a large lesion adjacent to the confluence of venous sinuses which may have influenced the perfusion fraction estimate. Similarly, a cutoff value for f_{90} of 15 has a sensitivity of 80% and specificity of 100%.

ADC did not differentiate tumor from pathological radiation necrosis ($ADC_{mean} = 1.1 \pm 0.2$ vs. 1.2 ± 0.4, $p = 0.6$; $ADC_{10} = 0.8 \pm 0.5$ vs. 0.8 ± 0.3, $p = 1.0$). The corresponding

Table 1 Clinical and treatment characteristics for all lesions

No. of tumor	Histology	Age (years)	Sex (M/F)	Location	Initial tumor size, largest dimension (cm)	Radiation dose (Gy/No. of fractions)	Time to progressive enhancement (months)	Predominant histopathology
1	Lung	50	F	Cerebellum	2.3	30 5	12	Pure radiation necrosis
2	Breast	50	F	Right occipital	2.0	20/1	14	Tumor
3	Lung	53	M	Left frontal	1.3	18/1	26	Radiation necrosis
4	Rectal	71	M	Cerebellum	3.5	35 5	7	Radiation necrosis
5	Breast	65	F	Right frontal	2.6	24/3	7	Radiation necrosis
6	Breast	72	F	Left frontal	0.7	20/1	16	Tumor
7	Lung	49	F	Right frontal	2.3	30/5	8	Tumor
8	Lung	56	F	Left frontal	1.6	30/5	13	Radiation necrosis
9	Melanoma	25	M	Left frontal	2.2	30/5	6	Tumor
10	Melanoma	25	M	Right frontal	2.2	27.5/5	9	Tumor

mean and histogram analysis for ADC and perfusion fraction for recurrent tumor and radiation necrosis are shown in Figs. 3 and 4.

Discussion

This study demonstrates the potential utility of the IVIM perfusion fraction to differentiate tumor from radiation necrosis in patients with brain metastases treated with high dose stereotactic radiation. To our knowledge this is the first study that evaluates IVIM parameters with histopathologic confirmation for brain metastases.

Surgical resection of irradiated lesions is typically reserved for the most complex cases with the greatest uncertainty regarding the diagnosis of necrosis or recurrent tumor. Previous small series of patients have reported histological rates of pure radiation necrosis after resection between 5 and 33%, with remaining cases composed of a mix of necrosis and residual tumor [8, 18, 28–30]. None of these studies, however, report the relative proportion of necrosis and viable tumor in cases where they are both present, and do not differentiate tumor necrosis from radiation necrosis. In the most comprehensive description of pathological features of resected brain metastases after SRS, Szeifert et al. report that in 13 of 18 cases (72%), small islands of residual tumor cells were present occupying up to 5% of the histological volume of tissue, but it is not known if these cells have further proliferative potential [26]. The difficulty in using conventional MRI to differentiate radiation necrosis from recurrent tumor was shown in a study using directed biopsies of a progressive region of enhancement of 14 brain metastases after radiation: eight lesions exhibited recurrent tumor cells while the remaining six were composed of radiation necrosis [31].

A previous study by Kim et al. demonstrated that IVIM can be used to distinguish recurrent tumor from treatment effects in a cohort of 91 patients using longitudinal imaging follow-up to determine outcomes [20]. In contrast the present study uses the more reliable reference standard of surgical pathology. In the study by Kim et al., perfusion fraction had a better diagnostic performance than ADC and CBV (derived from DSC perfusion MRI), but the combination of all three parameters had the highest diagnostic performance [20]. In the current study the ADC was not predictive in differentiating tumor from pathological radiation necrosis. The absolute values for perfusion fraction in our study for both recurrent tumor ($f_{90}=19.8$) and radiation necrosis ($f_{90}=14.9$) were higher than the values in the study by Kim ($f_{90,\ tumor}=7.9$ and $f_{90,\ necrosis}=4.8$). However, other published data reports the mean perfusion fraction in gliomas and brain metastases of 10–15 [21] in keeping with the values observed in our study. The differences between the linear regression model used in this study and the biexponential model used by Kim et al. may account for some, but likely not all, of the differences in perfusion fraction values. Additionally, a possible explanation lies in differences in the patient populations; this study included cases with the greatest uncertainty regarding the underlying pathology which led to the decision to pursue surgical excision while the study by Kim et al. presumably had more cases of pure radiation necrosis leading to lower perfusion fractions. This hypothesis is supported by the complex mix of histologies seen in the excised surgical specimens in this

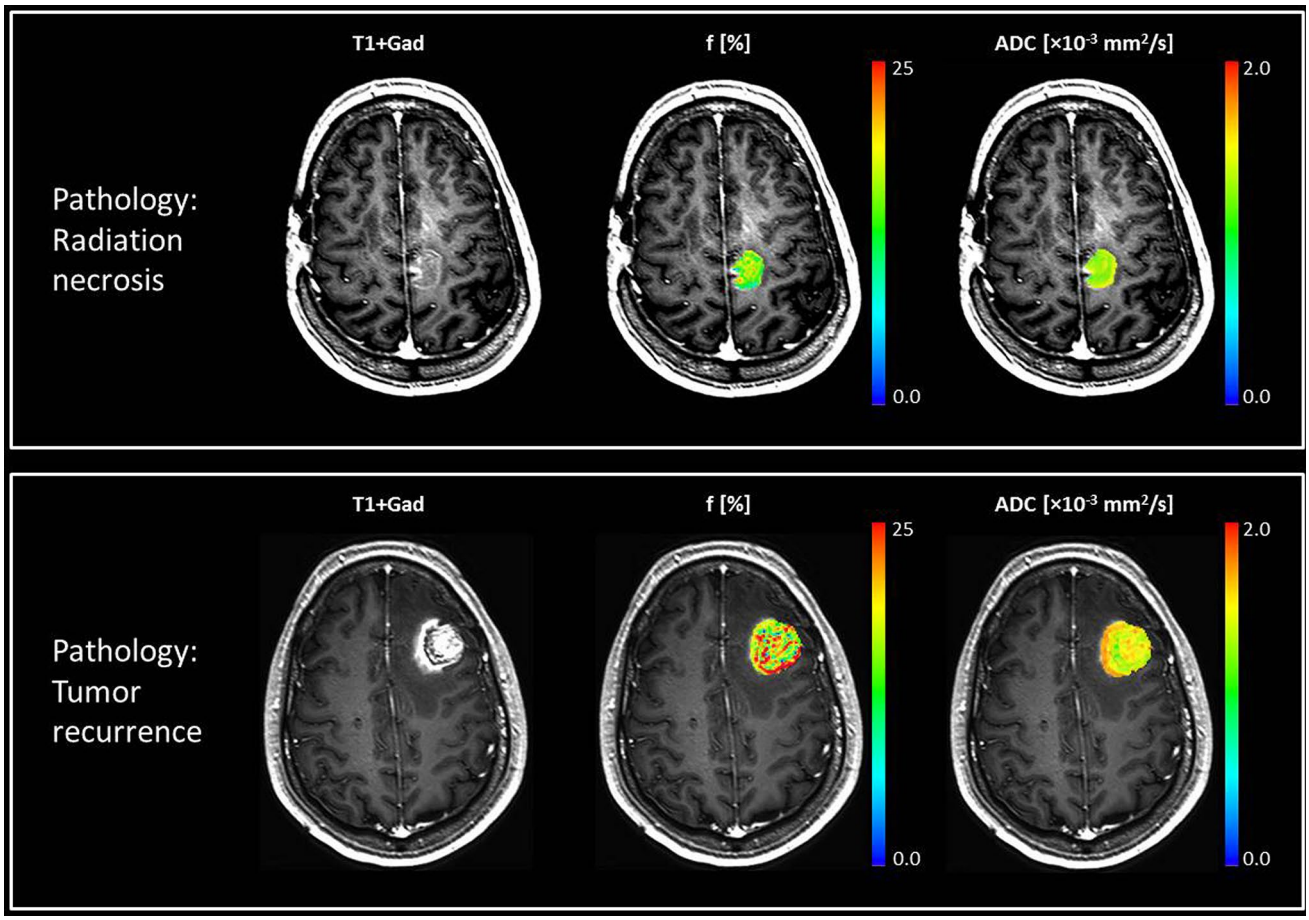

Fig. 1 Anatomical post-Gadolinium T1-weighted images (*left*), perfusion fraction f-map (*middle*), and ADC map (*right*) for a case of radiation necrosis (*top row*) and recurrent tumor (*bottom row*). The case of radiation necrosis exhibits a uniformly low perfusion fraction ($f_{mean}=7.7$, $f_{90}=13.6$) while the recurrent tumor is more heterogeneous with a higher perfusion fraction ($f_{mean}=10.9$, $f_{90}=21.8$). For this case the ADCs were similar but slightly higher for radiation necrosis ($ADC_{mean}=0.7$, $ADC_{10}=0.5$) than for recurrent tumor ($ADC_{mean}=1.1$, $ADC_{10}=0.7$)

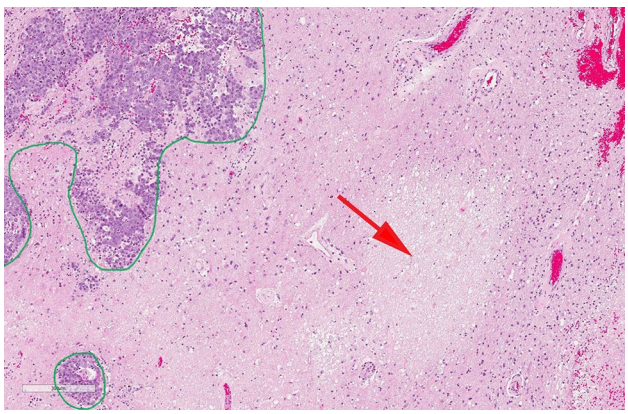

Fig. 2 H&E stain of a resected recurrent brain metastasis showing a region of residual viable tumor (outlined in *green*) next to a small area of bland radiation necrosis (*red arrow*)

study. The absolute values for ADC were similar between the two studies.

Previous reports have shown DSC perfusion [13] and diffusion [32, 33] imaging as promising methods for differentiating tumor from necrosis in gliomas and brain metastases. IVIM perfusion fraction and DSC-derived CBV are similar but not necessarily identical measures of perfusion. Studies have conflicting conclusions about the degree of correlation between perfusion fraction and CBV [34, 35]. DSC is susceptible to contamination of its signal from blood flow from larger arteries and veins while IVIM is inherently most sensitive to flow within the microcirculation. This is supported by direct comparison of IVIM to histopathologic microvessel density in animal models [36, 37]. Other strengths of IVIM include the lack of intravenous contrast administration which would allow for multiple perfusion measurements in order to better understand the temporal evolution of perfusion after radiation in future

Table 2 Individual lesion perfusion parameters and associated tumor fraction

No. of tumor	Mean f (%)	f_{90} (%)	STD f	Mean ADC (10^{-3} mm^2/s)	ADC_{10} (10^{-3} mm^2/s)	STD ADC	Histological tumor fraction (%)
1	8.6	16.2	5.7	1.3	0.9	0.3	0
2	9.5	13.9	4.3	1.2	0.9	0.3	45
3	7.7	13.6	4.7	0.7	0.5	0.2	20
4	9.8	15.1	5.1	1.5	1.2	0.3	5
5	8.6	18.1	6.8	1.6	0.9	0.5	5
6	10.4	23.3	8.2	1.1	0.7	0.3	30
7	10.3	18.3	6	1.2	0.9	0.2	40
8	6.6	11.6	3.9	0.8	0.6	0.1	20
9	10.9	21.8	7.8	1.1	0.7	0.3	30
10	9.3	21.7	8.1	0.7	0.2	0.4	50

F perfusion fraction, f_{90} 90th percentile for f, *STD* standard deviation, *ADC* apparent diffusion coefficient, ADC_{10} 10th percentile for ADC

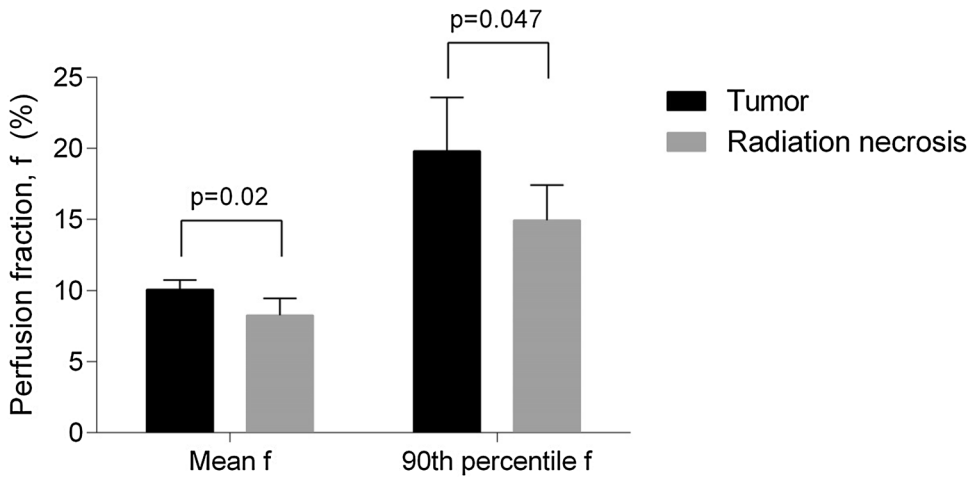

Fig. 3 Mean and 90th percentile perfusion fraction (f) for recurrent tumors versus radiation necrosis

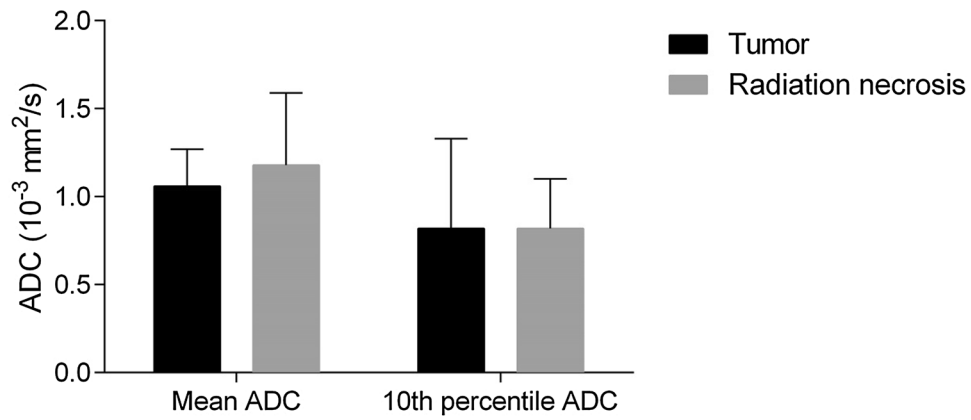

Fig. 4 Mean and 10th percentile apparent diffusion coefficient (ADC) for recurrent tumor versus radiation necrosis

studies. IVIM allows for inherent co-registration between diffusion and perfusion parameters facilitating multi-parametric analysis. Unlike IVIM, DSC perfusion analysis typically requires more complicated mathematical modeling and the use of a user-defined arterial input function and a region of contralateral unaffected white matter.

These results illustrate that, like the biexponential model [20], the simplified IVIM-derived perfusion fraction using linear regression can distinguish tumor from pathological radiation necrosis. The advantage of the simplified IVIM model is that the number of b-values in the DWI acquisition (and subsequent overall scan time) can be limited. It

has recently been demonstrated that an accurate measurement of perfusion fraction can be obtained with as few as two b-values using this simplified model [24]. In normal brain, the linear model has been shown to have a higher correlation with CBV than the biexponential model [38], likely due to the higher sensitivity of the biexponential model to noise [39]. Recent consensus guidelines advise that standard brain tumor imaging with MRI include a DWI acquisition with two b-values (500 and 1000 s/mm^2) [40]. This would allow for widespread adoption of IVIM-based perfusion and diffusion parameters as a method to characterize brain metastases before and after treatment and would facilitate the ongoing study of these imaging biomarkers and their relationship to outcomes. The current study only requires contouring of enhancing regions on a post-Gadolinium T1-weighted image and not any visual determination of areas of potential recurrence on perfusion maps themselves. This would also enable widespread adoption of IVIM perfusion imaging across institutions and vendors.

We recognize that a multi-parametric analysis will likely provide the most robust characterization of irradiated brain metastases to guide treatment decisions. This study and the results from Kim et al. [20] suggest that IVIM perfusion imaging should be included in future imaging studies of patients with brain metastases treated with radiation. The complex nature of enlarging enhancing disease after SRS is demonstrated by the mix of histopathologies in these ten lesions, illustrating the difficulty of using biopsies or longitudinal imaging follow up as a gold standard for determining outcomes in patients with brain metastases, particularly because attrition is high in this cohort of patients. Further validation in a larger population cohort with histopathological correlation would be beneficial but likely require cooperation between multiple institutions.

This study has several limitations. The small number of patients means that further prospective study is warranted before definitive conclusions can be made about the utility of IVIM in differentiating tumor from pathological radiation necrosis after SRS treatment. There is no consensus definition of radiation necrosis on histopathology or on serial imaging follow-up, which hampers comparisons across trials. For this study we adopted a definition from a study by Tihan et al. [27] used to evaluate radiation necrosis of gliomas, however, this definition is not standard or validated and it is not clear if a different histopathological definition should be used for brain metastases.

Conclusion

In this study, IVIM was useful in distinguishing tumor from pathological radiation necrosis in patients with brain metastases treated with SRS. These findings need to be validated in a larger cohort as this was an exploratory, hypothesis-generating study with a limited sample size. Accurate imaging biomarkers may allow for a more rapid decision to pursue salvage surgery for recurrent tumor or more confidence in following with observation and medical management for regions of radiation necrosis.

Compliance with ethical standards

Conflict of interest The authors declare that they have no conflict of interest.

References

1. Linskey ME, Andrews DW, Asher AL, Burri SH, Kondziolka D, Robinson PD, Ammirati M, Cobbs CS, Gaspar LE, Loeffler JS, McDermott M, Mehta MP, Mikkelsen T, Olson JJ, Paleologos NA, Patchell RA, Ryken TC, Kalkanis SN (2010) The role of stereotactic radiosurgery in the management of patients with newly diagnosed brain metastases: a systematic review and evidence-based clinical practice guideline. J Neurooncol 96:45–68. doi:10.1007/s11060-009-0073-4
2. Chang EL, Wefel JS, Hess KR, Allen PK, Lang FF, Kornguth DG, Arbuckle RB, Swint JM, Shiu AS, Maor MH, Meyers CA (2009) Neurocognition in patients with brain metastases treated with radiosurgery or radiosurgery plus whole-brain irradiation: a randomised controlled trial. Lancet Oncol 10:1037–1044. doi:10.1016/S1470-2045(09)70263-3
3. Soliman H, Das S, Larson DA, Sahgal A (2016) Stereotactic radiosurgery (SRS) in the modern management of patients with brain metastases. Oncotarget. doi:10.18632/oncotarget.7131
4. Chao ST, Ahluwalia MS, Barnett GH, Stevens GHJ, Murphy ES, Stockham AL, Shiue K, Suh JH (2013) Challenges with the diagnosis and treatment of cerebral radiation necrosis. Int J Radiat Oncol Biol Phys 87:449–457. doi:10.1016/j.ijrobp.2013.05.015
5. Le Rhun E, Dhermain F, Vogin G, Reyns N, Metellus P (2016) Radionecrosis after stereotactic radiotherapy for brain metastases. Expert Rev Neurother 16:1–12. doi:10.1080/14737175.2016.1184572
6. Parvez K, Parvez A, Zadeh G (2014) The diagnosis and treatment of pseudoprogression, radiation necrosis and brain tumor recurrence. Int J Mol Sci 15:11832–11846. doi:10.3390/ijms150711832
7. Kohutek ZA, Yamada Y, Chan TA, Brennan CW, Tabar V, Gutin PH, Jonathan Yang T, Rosenblum MK, Ballangrud A, Young RJ, Zhang Z, Beal K (2015) Long-term risk of radionecrosis and imaging changes after stereotactic radiosurgery for brain metastases. J Neurooncol 125:149–156. doi:10.1007/s11060-015-1881-3
8. Truong MT, St Clair EG, Donahue BR, Rush SC, Miller DC, Formenti SC, Knopp EA, Han K, Golfinos JG (2006) Results of surgical resection for progression of brain metastases previously treated by gamma knife radiosurgery. Neurosurgery 59:86–97. doi:10.1227/01.NEU.0000219858.80351.38
9. Levin VA, Bidaut L, Hou P, Kumar AJ, Wefel JS, Bekele N, Grewal J, Prabhu S, Loghin M, Gilbert MR, Jackson EF (2012) Randomized double-blind placebo-controlled trial of bevacizumab therapy for radiation necrosis of the central nervous system. Int J Radiat Oncol Biol Phys 79:1487–1495. doi:10.1016/j.ijrobp.2009.12.061.Randomized

10. Dequesada IM, Quisling RG, Yachnis A, Friedman WA (2008) Can standard magnetic resonance imaging reliably distinguish recurrent tumor from radiation necrosis after radiosurgery for brain metastases? A radiographic-pathological study. Neurosurgery 63:898–903. doi:10.1227/01.NEU.0000333263.31870.31
11. Hein PA, Eskey CJ, Dunn JF, Hug EB (2004) Diffusion-weighted imaging in the follow-up of treated high-grade gliomas: tumor recurrence versus radiation injury. Am J Neuroradiol 25:201–209
12. Bisdas S, Naegele T, Ritz R, Dimostheni A, Pfannenberg C, Reimold M, Koh TS, Ernemann U (2011) Distinguishing recurrent high-grade gliomas from radiation injury. A pilot study using dynamic contrast-enhanced MR imaging. Acad Radiol 18:575–583. doi:10.1016/j.acra.2011.01.018
13. Barajas RF, Chang JS, Sneed PK, Segal MR, McDermott MW, Cha S (2009) Distinguishing recurrent intra-axial metastatic tumor from radiation necrosis following gamma knife radiosurgery using dynamic susceptibility—weighted contrast-enhanced perfusion MR imaging. Am J Neuroradiol 30:367–372. doi:10.3174/ajnr.A1362
14. Schlemmer HP, Bachert P, Henze M, Buslei R, Herfarth KK, Debus J, van Kaick G (2002) Differentiation of radiation necrosis from tumor progression using proton magnetic resonance spectroscopy. Neuroradiology 44:216–222. doi:10.1007/s002340100703
15. Tie J, Gunawardana DH, Rosenthal MA (2008) Differentiation of tumor recurrence from radiation necrosis in high-grade gliomas using 201Tl-SPECT. J Clin Neurosci 15:1327–1334. doi:10.1016/j.jocn.2007.12.008
16. Di Chiro G, Oldfield E, Wright DC, Demichele D, Katz DA, Patronas NJ, Doppman JL, Larson SM, Ito M, Kufta CV (1988) Cerebral necrosis after radiotherapy and or intraarterial chemotherapy for brain-tumors—pet and neuropathologic studies. Am J Roentgenol 150:189–197. doi:10.2214/ajr.150.1.189
17. Terakawa Y, Tsuyuguchi N, Iwai Y, Yamanaka K, Higashiyama S, Takami T, Ohata K (2008) Diagnostic accuracy of 11 C-methionine PET for differentiation of recurrent brain tumors from radiation necrosis after radiotherapy. J Nucl Med 49:694–699. doi:10.2967/jnumed.107.048082
18. Telera S, Fabi A, Pace A, Vidiri A, Anelli V, Carapella CM, Marucci L, Crispo F, Sperduti I, Pompili A (2013) Radionecrosis induced by stereotactic radiosurgery of brain metastases: results of surgery and outcome of disease. J Neurooncol 113:313–325. doi:10.1007/s11060-013-1120-8
19. Le Bihan D, Breton E, Lallemand D, Grenier P, Cabanis E, Laval-Jeantet M (1986) MR imaging of intravoxel incoherent motions: application to diffusion and perfusion in neurologic disorders. Radiology 161:401–407. doi:10.1148/radiology.161.2.3763909
20. Kim DY, Kim HS, Goh MJ, Choi CG, Kim SJ (2014) Utility of intravoxel incoherent motion MR imaging for distinguishing recurrent metastatic tumor from treatment effect following gamma knife radiosurgery: initial experience. Am J Neuroradiol 35:2082–2090. doi:10.3174/ajnr.A3995
21. Federau C, O'Brien K, Meuli R, Hagmann P, Maeder P (2014) Measuring brain perfusion with intravoxel incoherent motion (IVIM): initial clinical experience. J Magn Reson Imaging 39:624–632. doi:10.1002/jmri.24195
22. Turner R, Le Bihan D, Maier J, Vavrek R, Hedges LK, Pekar J (1990) Echo-planar imaging of intravoxel incoherent motion. Radiology 177:407–414. doi:10.1148/radiology.177.2.2217777
23. Le Bihan D (1988) Intravoxel incoherent motion imaging using steady-state free precession. Magn Reson Med 7:346–351
24. Conklin J, Heyn C, Roux M, Cerny M, Wintermark M, Federau C (2016) A simplified model for intravoxel incoherent motion perfusion imaging of the brain. Am J Neuroradiol 37:2251–2257. doi:10.3174/ajnr.A4929
25. Kim HS, Suh CH, Kim N, Choi CG, Kim SJ (2014) Histogram analysis of intravoxel incoherent motion for differentiating recurrent tumor from treatment effect in patients with glioblastoma: initial clinical experience. Am J Neuroradiol 35:490–497. doi:10.3174/ajnr.A3719
26. Szeifert GT, Atteberry DS, Kondziolka D, Levivier M, Lunsford LD (2006) Cerebral metastases pathology after radiosurgery: a multicenter study. Cancer 106:2672–2681. doi:10.1002/cncr.21946
27. Tihan T, Barletta J, Parney I, Lamborn K, Sneed PK, Chang S (2006) Prognostic value of detecting recurrent glioblastoma multiforme in surgical specimens from patients after radiotherapy: should pathology evaluation alter treatment decisions? Hum Pathol 37:272–282
28. Williams BJ, Suki D, Fox BD, Pelloski CE, Maldaun MVC, Sawaya RE, Lang FF, Rao G (2009) Stereotactic radiosurgery for metastatic brain tumors: a comprehensive review of complications. J Neurosurg 111:439–448. doi:10.3171/2008.11.JNS08984
29. Jagannathan J, Bourne TD, Schlesinger D, Yen C-P, Shaffrey ME, Laws ER, Sheehan JP (2010) Clinical and pathological characteristics of brain metastasis resected after failed radiosurgery. Neurosurgery 66:208–217. doi:10.1227/01.NEU.0000359318.90478.69
30. Vecil GG, Suki D, Maldaun MVC, Lang FF, Sawaya R (2005) Resection of brain metastases previously treated with stereotactic radiosurgery. J Neurosurg 102:209–215. doi:10.3171/jns.2005.102.2.0209
31. Alomari A, Rauch PJ, Orsaria M, Minja FJ, Chiang VL, Vortmeyer AO (2014) Radiologic and histologic consequences of radiosurgery for brain tumors. J Neurooncol 117:33–42. doi:10.1007/s11060-014-1359-8
32. Provenzale JM, Mukundan S, Barboriak DP (2006) Diffusion-weighted and perfusion MR imaging for brain tumor characterization and assessment of treatment response. Radiology 239:632–649. doi:10.1148/radiol.2393042031
33. Al Sayyari A, Buckley R, McHenery C, Pannek K, Coulthard A, Rose S (2010) Distinguishing recurrent primary brain tumor from radiation injury: a preliminary study using a susceptibility-weighted MR imaging-guided apparent diffusion coefficient analysis strategy. Am J Neuroradiol 31:1049–1054. doi:10.3174/ajnr.A2011
34. Federau C, Meuli R, O'Brien K, Maeder P, Hagmann P (2014) Perfusion measurement in brain gliomas with intravoxel incoherent motion MRI. Am J Neuroradiol 35:256–262. doi:10.3174/ajnr.A3686
35. Bisdas S, Braun C, Skardelly M, Schittenhelm J, Teo TH, Thng CH, Klose U, Koh TS (2014) Correlative assessment of tumor microcirculation using contrast-enhanced perfusion MRI and intravoxel incoherent motion diffusion-weighted MRI: is there a link between them? NMR Biomed 27:1184–1191. doi:10.1002/nbm.3172
36. Lee HJ, Rha SY, Chung YE, Shim HS, Kim YJ, Hur J, Hong YJ, Choi BW (2014) Tumor perfusion-related parameter of diffusion-weighted magnetic resonance imaging: correlation with histological microvessel density. Magn Reson Med 71:1554–1558. doi:10.1002/mrm.24810
37. Iima M, Reynaud O, Tsurugizawa T, Ciobanu L, Li JR, Geffroy F, Djemai B, Umehana M, Le Bihan D (2014) Characterization of glioma microcirculation and tissue features using intravoxel incoherent motion magnetic resonance imaging in a rat brain model. Investig Radiol 49:485–490. doi:10.1097/RLI.0000000000000040
38. Wirestam R, Borg M, Brockstedt S, Lindgren A, Holtas S, Stahlberg F (2001) Perfusion-related parameters in intravoxel incoherent motion MR imaging compared with CBV and CBF measured

by dynamic susceptibility-contrast MR technique. Acta Radiol 42:123–128
39. Pekar J, Moonen CT, van Zijl PC (1992) On the precision of diffusion/perfusion imaging by gradient sensitization. Magn Reson Med 23:122–129
40. Ellingson BM, Bendszus M, Boxerman J, Barboriak D, Erickson BJ, Smits M, Nelson SJ, Gerstner E, Alexander B, Goldmacher G, Wick W, Vogelbaum M, Weller M, Galanis E, Kalpathy-Cramer J, Shankar L, Jacobs P, Pope WB, Yang D, Chung C, Knopp MV, Cha S, van den Bent MJ, Chang S, Yung WK, Cloughesy TF, Wen PY, Gilbert MR (2015) Consensus recommendations for a standardized brain tumor imaging protocol in clinical trials. Neuro Oncol 17:1188–1198. doi:10.1093/neuonc/nov095